Effects of Geometric Parameters on Performance of Rectangular Submerged Inlet for Aircraft

LIU Chao[1*], *PEI Houju*[1], *CHEN Changdong*[2], *XU Wenbing*[3], *YANG Kaijie*[4]

1. Environment Control and Oxygen System Department, Shanghai Aircraft Design and Research Institute, Shanghai 201210, P. R. China;

2. AVIC Nanjing Servo Control System Corporation, Nanjing 210016, P. R. China;

3. College of Energy & Power Engineering, Jiangsu University of Science and Technology, Zhenjiang 212003, P. R. China;

4. Key Laboratory of Aircraft Environment Control and Life Support, MIIT, Nanjing University of Aeronautics and Astronautics, Nanjing 210016, P. R. China

(Received 6 September 2021; revised 23 September 2021; accepted 16 December 2021)

Abstract: To improve the comfortability and safety of aircraft, the demand of rectangular submerged inlets (RSIs) with low resistance is proposed to increase the inlet flow rate of ram air. A theoretical model is built to numerically analyze the effects of geometric parameters on the inlet mass flow rate of RSIs. The geometric parameters in question here encompass the aspect ratio of 2—4, the ramp angle of 6°—7°, the characteristic parameter of the throat of 0.20—0.30, the ramp length of 939—1 337 mm, and the cone angle of 0°—3°. Simulation results demonstrate that the mass flow rate (MFR) is positively correlated with the aspect ratio, ramp angle, ramp length, and cone angle, and negatively correlated with characteristic parameter of the throat. Within the range of the geometric parameters considered, the RSI with the aspect ratio of 3, the ramp angle of 6°, the characteristic parameter of the throat of 0.20, the ramp length of 1 337 mm, and the cone angle of 3° obtains the largest MFR value of about 2.251 kg/s.

Key words: ram air system; rectangular submerged inlet; geometric parameter; mass flow rate (MFR)

CLC number: V245.34 **Document code:** A **Article ID:** 1005-1120(2021)06-0984-09

0 Introduction

As an important part of the aircraft environment control system (ECS), the primary function of the ram air system (RAS) is to induce outside low-temperature air into ECS to cool electronic devices and provide increased comfort for passengers[1-2]. The performance of RAS depends on the geometry of the ram air inlet: Scoop-type inlet[3], national advisory committee for aeronautics (NACA) submerged inlet[4] and rectangular submerged inlet (RSI)[5]. Although more air can be induced, the scoop-type inlet increases the drags due to the protruded geometry from the fuselage[6-7]. RSI has a similar geometric configuration with NACA submerged inlet but differs in opening and side-walls shape. As indicated by its name, RSI is made up of a rectangular opening connected to the downstream duct. Compared with the scoop-type inlet, RSI has fewer drags but also less mass flow rate (MFR). Thus, it might be significant to explore the effect of geometric parameters on the performance of RSI and then obtain enough MFR and reduce drags.

Related research at home and abroad has primarily focused on NACA submerged inlet[8-13]. The influence of different shapes of side-walls on the ram air recovery ratio and drags has been studied experimentally by Taylor et al[8]. Mossman et al.[9] investigated the effect of three typical geometric parameters (i.e., aspect ratio, ramp angle, and ramp length) on the total pressure recovery in a wind tunnel. Holzhauser et al.[10] analyzed and compared the performance of large scale model and small scale model. Sun et al.[11] studied effects of entrance parameters (i.e., characteristic parameters of the aft lip, ramp angle, and side edge angle) on the perfor-

*Corresponding author, E-mail address: liuchao@comac.cc.

How to cite this article: LIU Chao, PEI Houju, CHEN Changdong, et al. Effects of geometric parameters on performance of rectangular submerged inlet for aircraft[J]. Transactions of Nanjing University of Aeronautics and Astronautics, 2021, 38(6): 984-992.

http://dx.doi.org/10.16356/j.1005-1120.2021.06.009

mance of a submerged inlet with flush-mounted planar side entrance. In recent years, many intelligent algorithms are also applied to optimize the performance of the NACA submerged inlet[14-16].

To date, much work has been done to study the effects of geometric parameters on total pressure recovery, ram ratio, drags and flow field distortion[17], and so on of the NACA submerged inlet and scoop-type inlet, but relatively few studies have been reported for RSI, especially with respect to MFR. With the development of wide-body aircraft, the demand for MFR on the plane keeps increasing. Thus, it is particularly important to study the influence of geometric parameters on MFR of the rectangular submerged inlet. The main purpose of this paper is to investigate the effects of geometric parameters on the performance of RSI. Based on a validated numerical method, effects of aspect ratio, ramp angle, characteristic parameter of the throat, ramp length, and cone angle on MFR are also being discussed. Generally, the results of this research may inform the design of RSIs for wide-body aircrafts.

1 Geometry Model and Numerical Method

1.1 Geometry model

The geometry model of RSI used in this paper is shown in Fig.1. As can be seen from Fig.1, RSI is usually located in the high-pressure area of the aircraft faring. When the air flows to the opening, a high dynamic flow is formed, which is induced into the downstream duct through the throat. The main design geometric parameters of RSI contain the aspect ratio A ($A=W/\mathrm{d}t$, where W is the throat width and $\mathrm{d}t$ the throat depth), ramp angle α, characteristic parameter of the throat B ($B=t/\mathrm{d}t$, where t is the lip height), ramp length L, and cone angle β. The parameters of the primary model are $A=4$, $\alpha=6°$, $B=0.20$, $L=1\,460$ mm, and $\beta=3°$, while various arrangements for different cases are presented in Table 1.

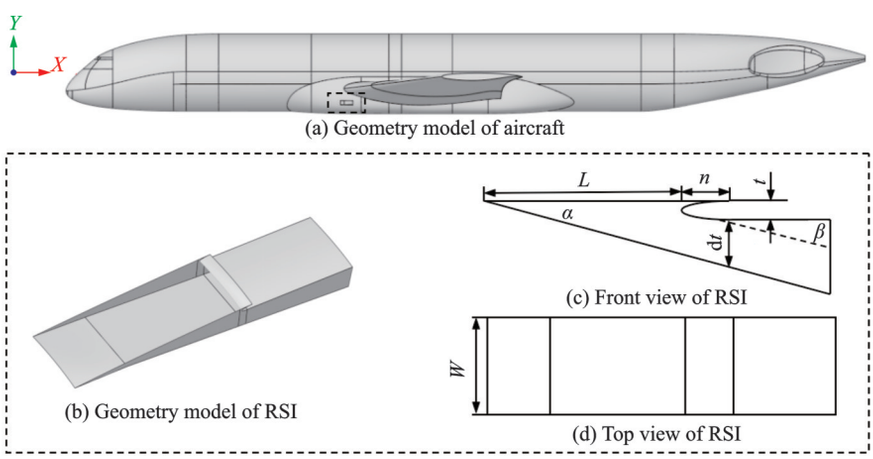

Fig.1 Schematic diagram of rectangular submerged inlet

Table 1 Value of different geometric parameters

Case	1	2	3	4	5
A	2, 3, 4	3	3	3	3
α/(°)	6	6,7,8	6	6	6
B	0.20	0.20	0.200 0.255 0.300	0.20	0.20
L /mm	939	939	939	939 1 138 1 337	939
β/(°)	3	3	3	3	0,2,3

1.2 Numerical method

1.2.1 Governing equations

Since the flow speed is much greater than 0.3 Mach (up to 0.85 Mach in present research work), it is justified to consider compressible effects.

For a compressible flow, the governing equations can be formulated as follows[18].

Continuity equation

$$\frac{\partial \rho}{\partial t}+\frac{\partial \rho u_i}{\partial x_i}=0 \tag{1}$$

Momentum equation

$$\frac{\partial \rho u_i}{\partial t}+\frac{\partial \rho u_i u_j}{\partial x_j}=-\frac{\partial p}{\partial x_i}+\frac{\partial \tau_{ij}}{\partial x_j} \tag{2}$$

Energy equation

$$\frac{\partial e}{\partial t}+\frac{\partial (e+p)u_j}{\partial x_j}=-\frac{\partial q_i}{\partial x_i}+\frac{\partial u_i \tau_{ij}}{\partial x_j} \tag{3}$$

where u_i and u_j are the velocities, ρ is the fluid density, q_i the heat flux, p the pressure and e the internal energy.

The flow is a three-dimensional, turbulent and steady-state flow. The commercial fluent dynamics software CFX 18.0 is used to solve the above three governing equations, which are discretized by the finite volume method (FVM). In the authors' previous works[14-15], the k-ε turbulence model used in numerical simulations has been validated. The solutions are considered being converged until the residual is less than 10^{-6} for all equations.

1.2.2 Fluid computational domain and boundary conditions

The computational domain and boundary conditions are shown in Fig.2. As can be seen from Fig.2, the boundary conditions of the fluid computational domain are mainly divided into Inlet, Outlet, Farwall, and SYM. The Inlet boundary is assumed to be a uniform velocity given the magnitude of 0.85 Mach and the attack angle of 2.5°. The Outlet boundary is assumed to be "Opening" with a reference pressure of 17 900 Pa and a temperature of 242.15 K. The Farwall boundary is assumed to be "Opening", in agreement with the parameter setting of Inlet. The SYM boundary is assumed to be "Symmetry". Besides, the fuselage and the RSI walls are assumed to be adiabatic (Zero heat flux) walls with zero velocities (No-slip condition), and the exit of RSI is set as "Opening" with a given pressure of 20 900 Pa.

1.2.3 Mesh and mesh independence validation

In this paper, a structured mesh generated by the commercial software ICEM is used for all simulations, as shown in Fig.3(a). The fluid computational domain is divided into three sub-zones: Far-field zone, fuselage zone, and RSI zone. The mesh of the far-field zone is coarse, and the fuselage and RSI zones are relatively fine, as shown in Fig.3(b).

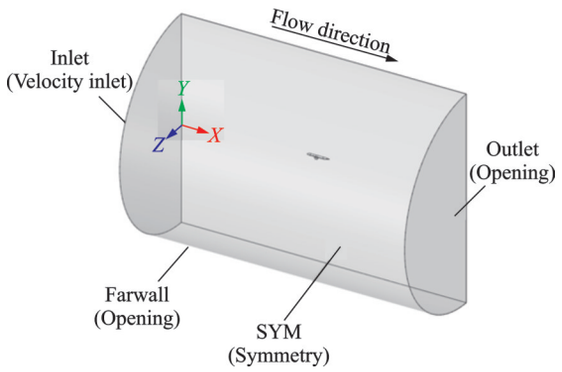

Fig.2 Fluid computational domain and boundary conditions

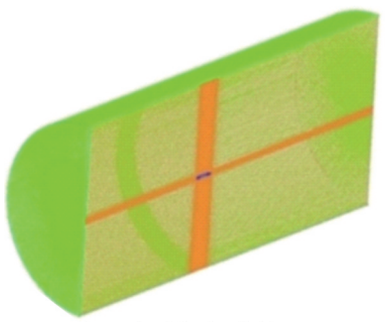

(a) Mesh of the far-field zone

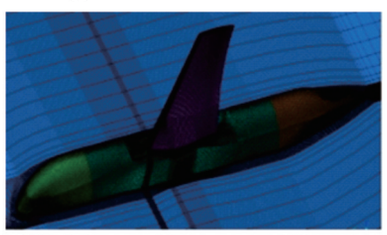

(b) Mesh around fuselage and RSI zones

Fig.3 Mesh details of the fluid computational domain

To balance the computational efficiency and accuracy, mesh independence validation is carried out to ensure that the final CFD solution is free of mesh resolution errors. Here taking the primary model as an illustration for mesh independence validation. Five mesh systems with 1.0×10^7, 1.5×10^7, 2.0×10^7, 2.5×10^7, 3.0×10^7 cells are chosen to compare MFR, and the results are shown in Fig.4. It is obvious that MFR changes by 0.04% from the grid size of 2.0×10^7 to 3.0×10^7. It shows that after the cells exceed 2.0×10^7, the changes in MFR can be neglected with a further increase in the number of cells. Thus, the mesh system of 2.0×10^7 cells is selected for the primary model.

1.2.4 Validation of the numerical method

Currently, there is no detailed experimental data on the performance research of the RSI. Thus,

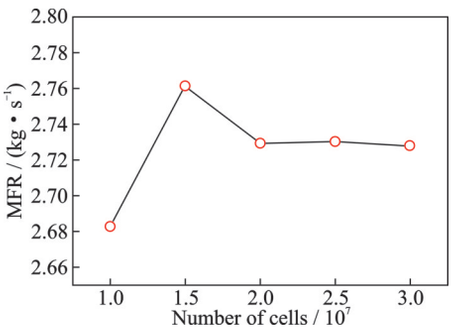

Fig.4 MFR under different numbers of cells

the numerical results of the NACA submerged inlet are compared with the wind tunnel test results to validate the reliability of the mesh resolution and the numerical method. The proposed numerical method in this paper is used for the simulations of the NACA submerged inlet, and the variation curve of ram pressure efficiency and mass flow rate is obtained. The ram pressure efficiency is calculated by[19]

$$\mathrm{RPE}=\frac{P_{t_{\mathrm{TH}}}-P_0}{P_{t_0}-P_0} \tag{4}$$

where $P_{t_{\mathrm{TH}}}$ is the total pressure at the throat plane, P_0 the static pressure of the free stream, and P_{t_0} the total pressure of the free stream.

All experiments are conducted in a 95 m-long, return-flow wind tunnel with a 2.4 m×2.4 m×9.6 m working section, and the experimental conditions are the same as the simulation conditions. The NACA submerged inlet is installed on a 1/7-scale model of a civil airplane, which is mainly composed of front fuselage, middle fuselage, wing body fairing, wing, ram air system, pressure measurement system, and so on. To ensure that the blockage ratio of the wind tunnel is not greater than 5%, the middle fuselage and wing are simplified. The upper surface of the middle fuselage is flattened, and the wing remains close to 1/4 of the total length of the wing. The installation diagram of the model in the wind tunnel is shown in Fig.5.

Simulation results are compared to experimental results in terms of ram pressure efficiency (RPE) and MFR at the exit of the NACA submerged inlet, as shown in Fig.6. As can be seen from Fig.6, simulation results are reasonably in agreement with experimental ones, and the maximum error is about

(a) Model of the civil aircraft

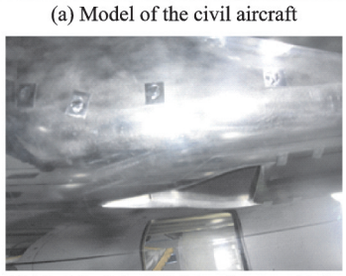

(b) Model of the NACA submerged inlet

Fig.5 Installation diagram of the model

3.5%. The results show that the proposed numerical method has high reliability and is suitable for subsequent research.

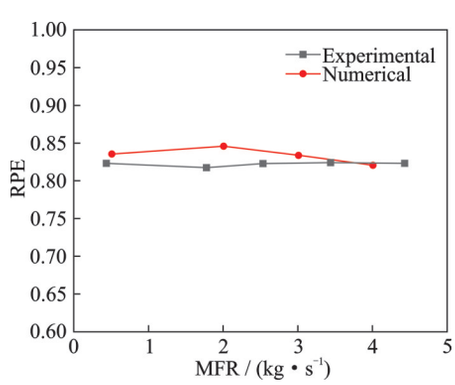

Fig.6 Comparison of numerical and experimental results

2 Influence of Geometric Parameters on MFR

2.1 Case 1: Influence of aspect ratio

Fig.7 shows the streamlines and velocity magnitude distributions at three different aspect ratios. As can be seen from Fig.7, the velocity magnitude distribution on the exit of RSI is uneven. There are two obvious low-velocity regions and one high-velocity region. The low-velocity regions are closed to the top center area and right bottom corner area, and the high-velocity region is located in the right side. The airflow is offset, showing that the velocity on the right side (i.e., the side near the bottom of the aircraft fairing) is large, while the velocity on

the left side is small. As the aspect ratio gradually increases, this phenomenon becomes more obvious. Further, the MFR for the exit of RSI at three different aspect ratios is given in Table 2. It is obvious that the MFR increases with the increase of aspect ratio. When the aspect ratio varies from 2 to 4, the MFR shows a drastic increase from 0.763 kg/s to 1.482 kg/s, by 94.2%.

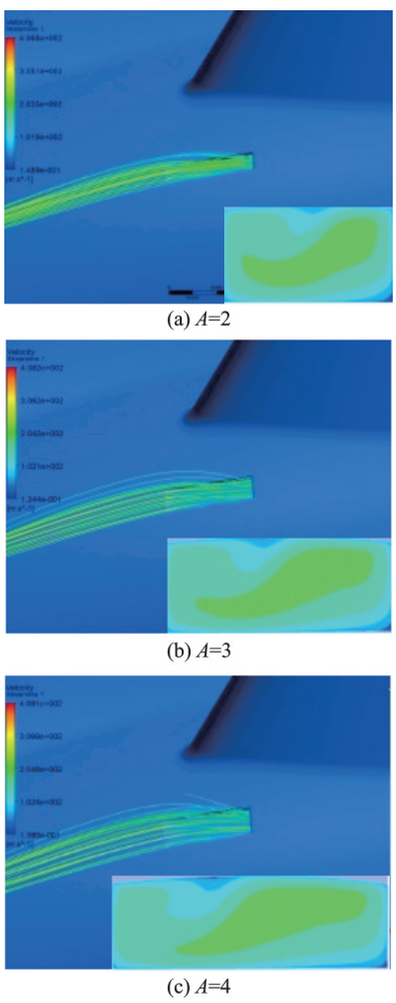

(a) A=2

(b) A=3

(c) A=4

Fig.7 Streamlines and velocity magnitude distribution at three different aspect ratios

Table 2 MFR at three different aspect ratios

A	2	3	4
MFR / (kg•s^{-1})	0.763	1.138	1.482

2.2 Case 2: Influence of ramp angle

The streamlines and velocity magnitude distributios at three different ram angles are shown in Fig.8. As can be seen from Fig.8, with the rise of ramp angle, the diffusion of streamlines becomes more apparent and more air flows into the RSI. No obvious offset occurs of the top center low-velocity region, but the area of this region is gradually reduced. At the same time, the velocity of this region is gradually increased. Further more, the MFR for the exit of RSI at three different ramp angles is given in Table 3. It is clear that the MFR increases with the rise of ramp angle. When the ramp angle varies from 6° to 8°, the MFR shows a drastic increase from 1.138 kg/s to 2.013 kg/s, by 76.9%.

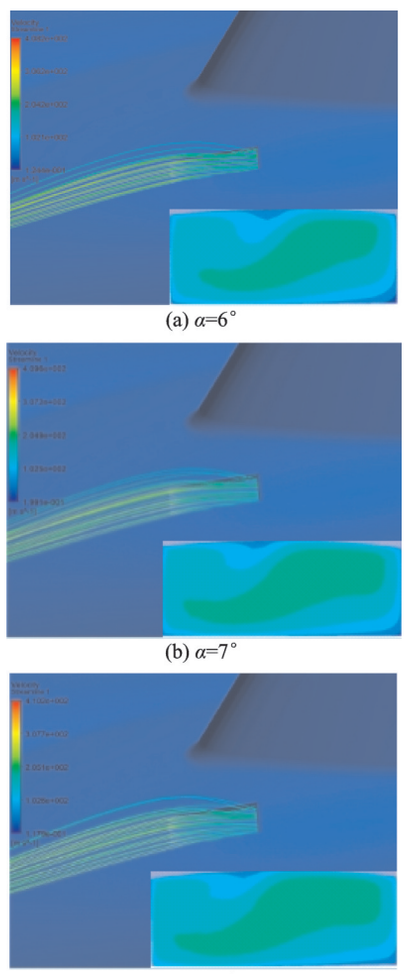

(a) α=6°

(b) α=7°

(c) α=8°

Fig.8 Streamlines and velocity magnitude distribution at three different ramp angles

Table 3 MFR at three different ramp angles

α/(°)	6	7	8
MFR/(kg•s^{-1})	1.138	1.541	2.013

2.3 Case 3: Influence of characteristic parameter of the throat

Fig.9 shows the streamlines and velocity mag-

nitude distributions at three different characteristic parameters of the throat. As can be seen from Fig.9, no significant change of streamlines of the airflow is observed. Further more, the MFR for the exit of RSI at three different characteristic parameters of the throat is given in Table 4. It is clear that the MFR decreases with the increase of characteristic parameter of the throat. When the characteristic parameter of the throat varies from 0.20 to 0.30, the MFR shows a slight decrease from 1.138 kg/s to 0.996 kg/s, by 12.5%.

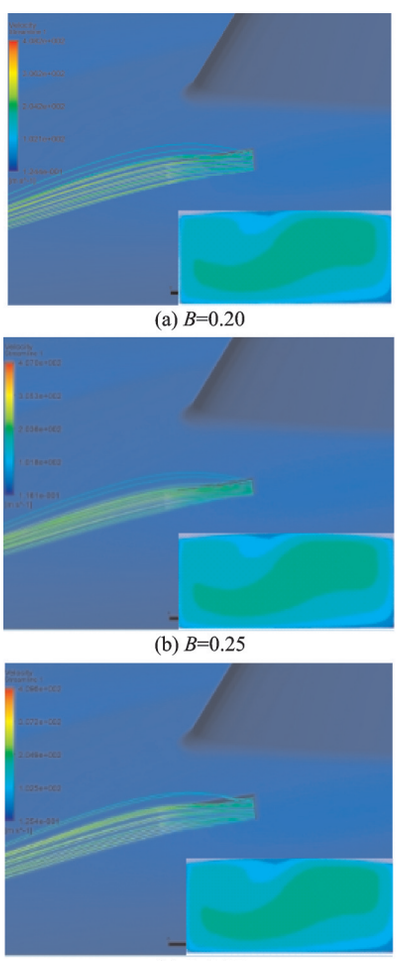

(a) B=0.20

(b) B=0.25

(c) B=0.30

Fig.9 Streamlines and velocity magnitude distribution at three different characteristic parameters of throat

Table 4 MFR at three different characteristic parameters of throat

B	0.20	0.25	0.30
MFR/(kg•s^{-1})	0.763	1.138	1.482

2.4 Case 4: Influence of ramp length

Fig.10 shows the streamlines and velocity magnitude distributions at three different ramp lengths. As shown in Fig.10, no significant change of the location of the top center low-velocity region is observed. Further more, the MFR for the exit of RSI at three different ramp lengths is given in Table 5. It is obvious that the MFR increases with the increase of ramp length. When the ramp length varies from 939 mm to 1 337 mm, the mass flow rate shows a drastic increase from 1.138 kg/s to 2.251 kg/s, by 97.8%.

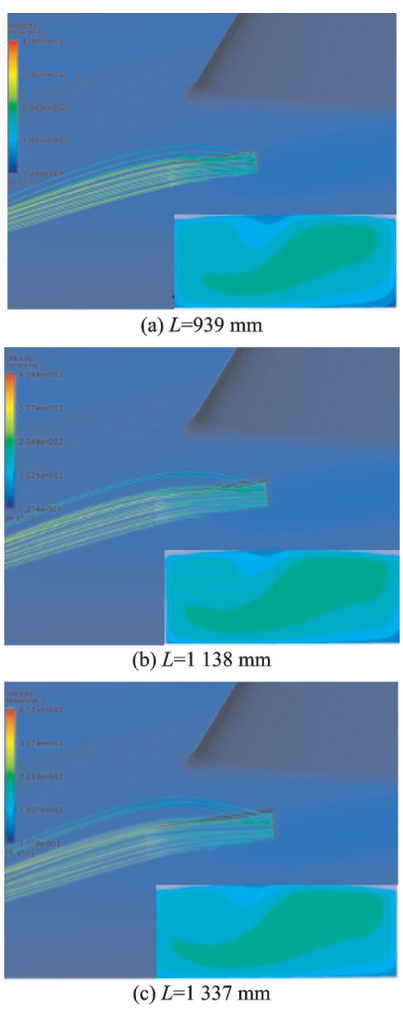

(a) L=939 mm

(b) L=1 138 mm

(c) L=1 337 mm

Fig.10 Streamlines and velocity magnitude distribution at three different ramp lengths

Table 5 MFR for three different ramp lengths

L/mm	939	1 138	1 337
MFR/(kg•s^{-1})	1.138	1.653	2.251

2.5 Case 5: Influence of cone angle

Fig.11 shows the streamlines and velocity magnitude distribution for three different cone angles. As shown in Fig.11, a slight diffusion of streamlines is observed and the MFR shows slight increase with the increase of cone angle. Further, the MFR for the exit of RSI at three different cone angles is given in Table 6. It is obvious that when the cone angle increases from 0° to 3°, the MFR increases only by 0.266 kg/s.

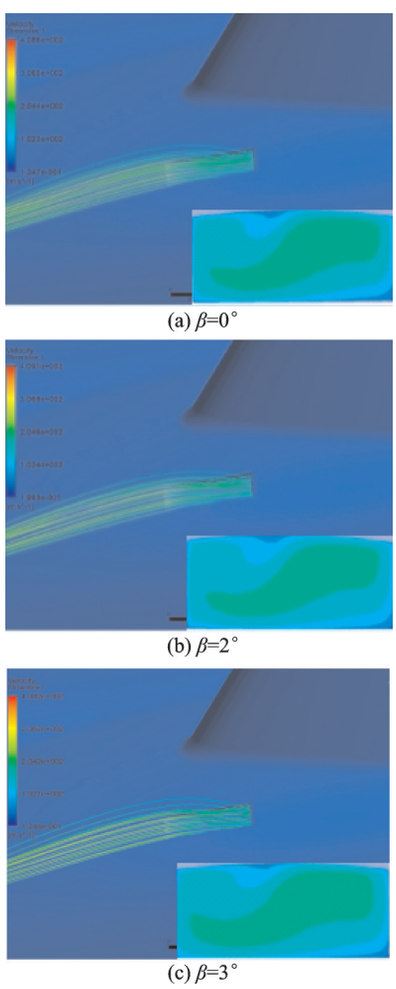

(a) β=0°

(b) β=2°

(c) β=3°

Fig.11 Streamlines and velocity magnitude distribution at three different cone angles

Table 6 MFR at three different cone angles

β/(°)	0	2	3
MFR/(kg•s^{-1})	0.872	1.067	1.138

3 Conclusions

Performance of the RSI is studied by three-dimension numerical simulations. Streamlines and velocity contour are provided to demonstrate MFR characteristics. The influence of aspect ratio, ramp angle, characteristic parameter of the throat, ramp length, and cone angle on MFR are investigated. The influence of diverse geometric parameters on MFR is also analyzed. The main conclusions can be drawn as follows.

(1) The RSI has the advantage for low drag compared with the scoop-type inlet and holds strong potential in performance enhancement of ECS. The velocity magnitude distribution on the exit of RSI is uneven. The airflow is offset, and then two obvious low-velocity regions appear at the top center area and right bottom corner area, and one high-velocity region appears at the right side. This phenomenon changes with the change of geometric parameters.

(2) MFR increases with aspect ratio, ramp angle, ramp length, and cone angle and decreases with characteristic parameter of the throat. Moreover, it shows a strong correlation with aspect ratio and ramp length, a moderate correlation with ramp angle, and a weak correlation with characteristic parameter of the throat and cone angle.

(3) Within the given range, MFR increases by 94.2% (A varies from 2 to 4), 76.9% (α varies from 6° to 8°), 97.8% (L varies from 939 mm to 1 337 mm) and 30.5% (β varies from 0° to 3°), respectively, and decreases by 12.5% (B varies from 0.20 to 0.30). Among considered geometric parameters and operating conditions, the RSI with A=3, α=6°, B=0.20, L=1 337 mm and β=3° obtains the largest MFR value of 2.251 kg/s.

References

[1] SHOU R Z, HE H S. Environment control for aircraft [M]. 1st ed. Beijing: Beijing University Press, 2004.

[2] WANG Y, LI Z M, PEI H J, et al. Research advances of ram air intake of civil aircraft[J]. Aviation Precision Manufacturing Technology, 2020, 56(1): 31-35, 39.

[3] HUANG G, SAHEBY E B, HAYS A. Propulsive efficiency of ridge/inlet configuration[J]. International Journal of Aerospace Engineering, 2018. DOI: 10.1155/2018/7462024.

[4] NICOLAS J, PIGNIER, CIARAN J O, et al. Aero-

dynamic and aeroacoustic analyses of a submerged air inlet in a low-Mach-number flow[J]. Computers & Fluids, 2016, 133: 15-31.

[5] SUN S, TAN H J, WANG C X. Submerged inlet performance enhancement using a unique bump-shaped vortex generator[J]. Journal of Propulsion and Power, 2016, 32(5): 1275-1280.

[6] ZENG L, PAN D, YE S, et al. A fast multi-objective optimization approach to S-duct scoop inlets design with both inflow and outflow[J]. Proceedings of the Institution of Mechanical Engineers, 2019, 233(9): 3381-3394.

[7] LIU L, SONG Y P, CHEN H L, et al. Design and optimization of half flush-mounted s-shaped inlet[J]. Journal of Propulsion Technology, 2014, 35(10): 1303-1309.

[8] TAYLOR R A. Some effects of side-wall modifications on the drag and pressure recovery of an NACA submerged inlet at transonic speeds: Technical Report Archive & Image Library[R]. [S.l.]: [s.n.], 1952.

[9] MOSSMAN E A, RANSALL L M. An experimental investigation of the design variables for NACA submerged duct entrances: The 1948 National Advisory Committee for Aeronautics research memorandum[R].[S.l.]:[s.n.], 1948.

[10] HOLZHAUSER C A, MARTIN N J. An experimental investigation at large scale of several configurations of an NACA submerged air intake: The 1948 National Advisory Committee for Aeronautics research memorandum[R].[S.l.]:[s.n.], 1948.

[11] SUN S, GUO R W, WU Y. Characterization and performance enhancement of submerged inlet with flush-mounted planar side entrance[J]. Journal of Propulsion & Power, 1971, 23(5): 987-995.

[12] LI Xuelai, REN Sanxing, WANG Qinfang, et al. On total pressure distortion of submerged intake[J]. Journal of Fuzhou University (Natural Science Edition), 2002, 30(2): 250-253, 257. (in Chinese)

[13] LIU Shaoyong, GUO Rongmei. Influence of throat parameters on performance of submerged inlet[J]. Journal of Nanjing University of Aeronautics & Astronautics, 2002, 34(1): 12-16. (in Chinese)

[14] PEI H J, CUI Y L, KONG B B, et al. Structural parameters optimization of submerged inlet using least squares support vector machines and improved genetic algorithm-particle swarm optimization approach[J]. Engineering Applications of Computational Fluid Mechanics, 2021, 15(1): 503-511.

[15] LI Z M, CHEN C D, PEI H J, et al. Structural optimization of the aircraft NACA inlet based on BP neural networks and genetic algorithms[J]. International Journal of Aerospace Engineering, 2020(2): 1-9.

[16] LOMBARDI A, FERRARI D, SANTOS L. Aircraft air inlet design optimization via surrogate-assisted evolutionary computation[C]//Proceedings of International Conference on Evolutionary Muti-criterion Optimization.[S.l.]: Springer, 2015: 313-327.

[17] JIN G L, SUK Y J, CHANG S A. Numerical simulation of three-dimensional flows for flush inlet[C]// Proceedings of the 22nd Applied Aerodynamics Conference and Exhibit. Providence: [s.n.], 2004: 1-5.

[18] LI Bo. Numerical simulation and noise control of compressible cavity flow[D]. Hefei: University of Science and Technology of China, 2020. (in Chinese)

[19] STEFAN K, RÜTTEN M, REIN M. Study of total pressure losses at the engine face of a submerged inlet with an ingested vortex[J]. New Results in Numerical and Experimental Fluid Mechanics Ⅺ, 2018, 136: 361-371.

Acknowledgement This work was supported by the Open Project of Key Laboratory of Aircraft Environment Control and Life Support, MIIT (No.KLAECLS-E-202001).

Author Mr. **LIU Chao** received the M.S. degree in man-machine-environment engineering from Nanjing University of Aeronautics and Astronautics, Nanjing, China, and obtained the title of Research Fellow in the Shanghai Aircraft Design and Research Institute, Environment Control and Oxygen System Department. His research is focused on environment control for aircraft.

Author contributions Mr. **LIU Chao** designed the study, complied the models, and conducted the analysis. Dr. **PEI Houju** interpreted the results and wrote the manuscript. Mr. **CHEN Changdong** contributed to the data and model components. Ms. **XU Wenbing** contributed to the analysis data. Mr. **YANG Kaijie** contributed to the discussion and background of the study. All authors commented on the manuscript draft and approved the submission.

Competing interests The authors declare no competing interests.

(Production Editor: WANG Jing)

矩形埋入式进气口结构参数对飞机性能的影响

刘　超[1], 裴后举[1], 陈常栋[2], 徐文冰[3], 杨凯杰[4]

(1. 上海飞机设计研究院环控氧气部,上海 201210,中国;
2. 中航工业南京伺服控制系统有限公司,南京 210016,中国;
3. 江苏科技大学能源与动力学院,镇江 212003,中国;
4. 南京航空航天大学飞行器环境控制与生命保障工业和信息化部重点实验室,南京 210016,中国)

摘 要:为了改善飞机的舒适性和安全性,提出一种低阻力的矩形埋入式进气口(Rectangular submerged inlets, RSIs)来提高冲压空气的进口流量,分析其主要结构参数并建立数值仿真模型。在此基础上,研究喉道宽高比(2～4)、斜坡倾角(6°～7°)、喉道特征比例(0.20～0.30)、开口长度(939～1 337 mm)和扩张角(0°～3°)这5个结构参数对矩形埋入式进气口质量流量(Mass flow rate, MFR)的影响情况。仿真结果表明:质量流量与喉道宽高比、斜坡倾角、开口长度和扩张角呈正相关,与喉道特征比例呈负相关。对于本研究,喉道宽高比为3、斜坡倾角α为6°、喉道特征比例为0.20、开口长度为1 337 mm,且扩张角为3°的进气口具有最大质量流量2.251 kg/s。

关键词:冲压空气系统;矩形埋入式进气口;结构参数;质量流量